Supplementary Information

Anomalous Diffusion of Targeted Carbon Nanotubes in Cellular Spheroids

Yichun Wang,[†‖] *Joong Hwan Bahng,*[†‖] *Quantong Che,*[‡] *Jishu Han,*[‡] *and Nicholas A. Kotov*[†‡,¶,‖,*]

[†]Department of Biomedical Engineering, University of Michigan, 3074 H.H. Dow Building, 2300 Hayward Street, Ann Arbor, MI 48109, USA, [‡]Department of Chemical Engineering, University of Michigan, 3074 H.H. Dow Building, 2300 Hayward Street, Ann Arbor, MI 48109, USA, [¶]Department of Material Science & Engineering, University of Michigan, 3074 H.H. Dow Building, 2300 Hayward Street, Ann Arbor, MI 48109, USA, [‖]Biointerfaces Institute, University of Michigan, North Campus Research Complex, 2800 Plymouth Rd, Ann Arbor, MI 48109, USA.

[*] Address correspondence to kotov@umich.edu

ADDITIONAL MATERIALS AND METHODS

Molecular Weight of CNTs and Their Derivatives. According to TEM images (**Figure S2.a**), the CNTs had an average diameter of 1.2 nm and a length of 1,000 nm. Therefore, it was calculated that 40 carbon atoms ((1.55 nm/0.245 nm) × (3.1414) × (2 carbon atoms)) are around the circumference. For every 0.283 nm length, there are 124 carbon atoms (4 x 40 carbons), namely, 6,790,106 amu ((1000nm/0.283nm) × (160) × (12.01)). So the calculated molecular weight of CNT is 6.79×10^6 Da. Fluorescent CNTs bearing, on average, 1-3 atomic % of FITC, which is 1246 Da (0.02 x 160 x 389.38 per tube) heavier than original CNTs as purchased (Figure S2.b). To determine how many antibodies are there on targeted CNT (CNT-TGFβ1-FITC), TEM images were captured and analyzed statistically and it was found 2~3 antibodies on each CNT in average,

which agreed with theoretical number 2.97 ± 0.32 (3.80×10^{-20} g, TGFβ1 MW 23000 Da × 1.66×10^{-24} g). As a result, the theoretical molecular weight of CNT-TGFβ1-FITC is 6.87×10^6 Da. The actual molecular weight was verified by TEM images and determined to be 6.84×10^6 Da due to loss during reaction (**Figure S2.c**).

ADDITIONAL DATA:

Available Biodistribution Data of CNT. CNTs have been realized as promising drug delivery and imaging vehicles because of their optical and electronic properties associated with quantum confinement. [2-11] However, numerous studies indicate that drug molecules have limited penetration into the interstitial space of a solid as reported for small-molecule chemotherapeutics [12-15] such as doxorubicin [16-20] and paclitaxel[21-24]. These drugs tend to be localized in regions surrounding blood vessels but do not further penetrate the internal part of the solid tumor, which represents a significant barrier to their efficacy [12]. In fact, the same barrier can be found for nanoparticles (NP) applied to drug delivery. Physical properties that control the penetration of molecules and particles into tissue include size, mass, charge, shape, and possibly others [25].

Considering these basic factors determining drug transport in tissues, NPs such as CNTs larger than 5–8 nm experience hindered diffusion compared to small molecules[26]. As a general rule, particles' diffusion rates decrease as particle size increases as a direct consequence of the fundamental laws of diffusion[27], which is not as ideal as small size-changing agents[28, 29]. However, CNTs are elongated particles with certain aspect ratios that can also affect diffusion rates[30] so that nanotubes were found to penetrate tumors more efficiently than spherical nanoparticles of the same effective hydrodynamic size[31]. This effect was attributed to nanotubes' alignment with the direction of interstitial fluid flow, which is expected to strongly increase the probability of passage through the interstitial gaps between the cells[32].

Additionally, the surface charge of penetrating species play a complex role in diffusion of drugs in tissues[33]. It is also strongly coupled with the circulation times and other pharmacokinetic parameters. Generally, neutral charge is better for interstitial transport in tumors[34] and long circulation times[35]. At the same time, the cationic charge optimizes trans-vascular transport in tumors [36]. Given these competing factors, the quantitative effect of charge on permeation of CNTs with functionalized group is incompletely understood and is likely to present unexpected dependencies. For instance, ligands modified CNTs could have distinguish properties on surface which lead the nanotubes interact with cells in tissue environment and therefore result in changed diffusion rate over the whole transportation.

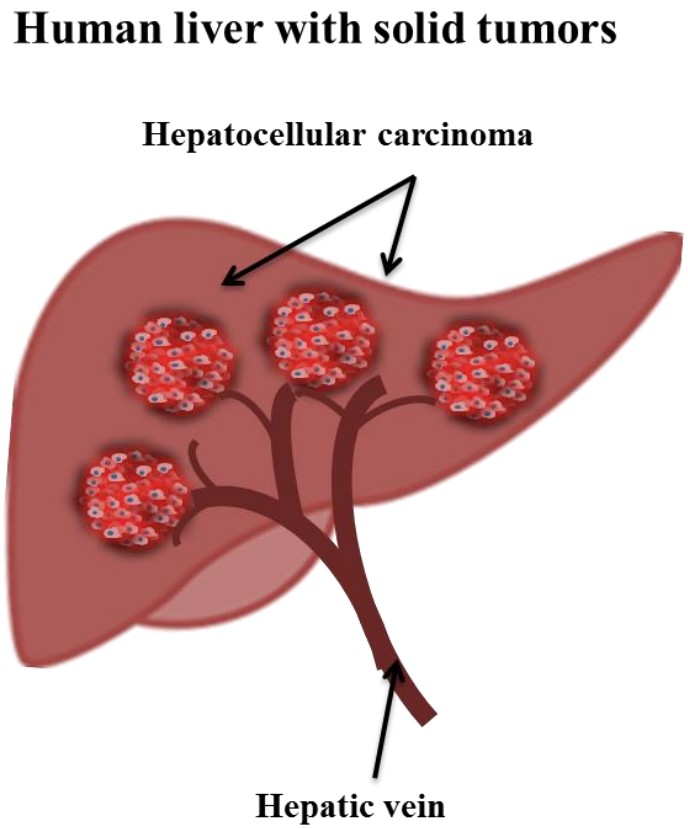

Figure S1. Hepatocellular carcinoma is one of most common solid tumors found in the human body and grows in human liver along branches of the hepatic vein.

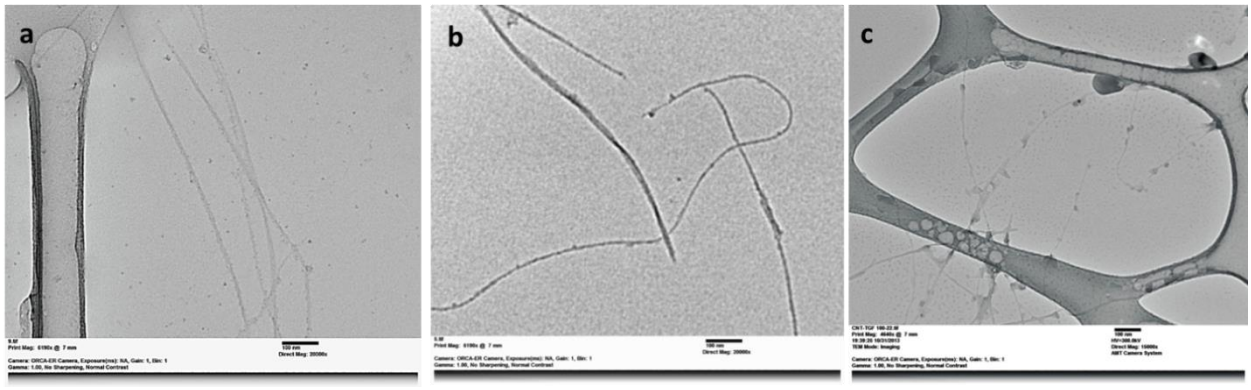

Figure S2. TEM images of CNT (**a**), CNT-FITC (**b**), and CNT-TGFβ1-FITC (**c**).

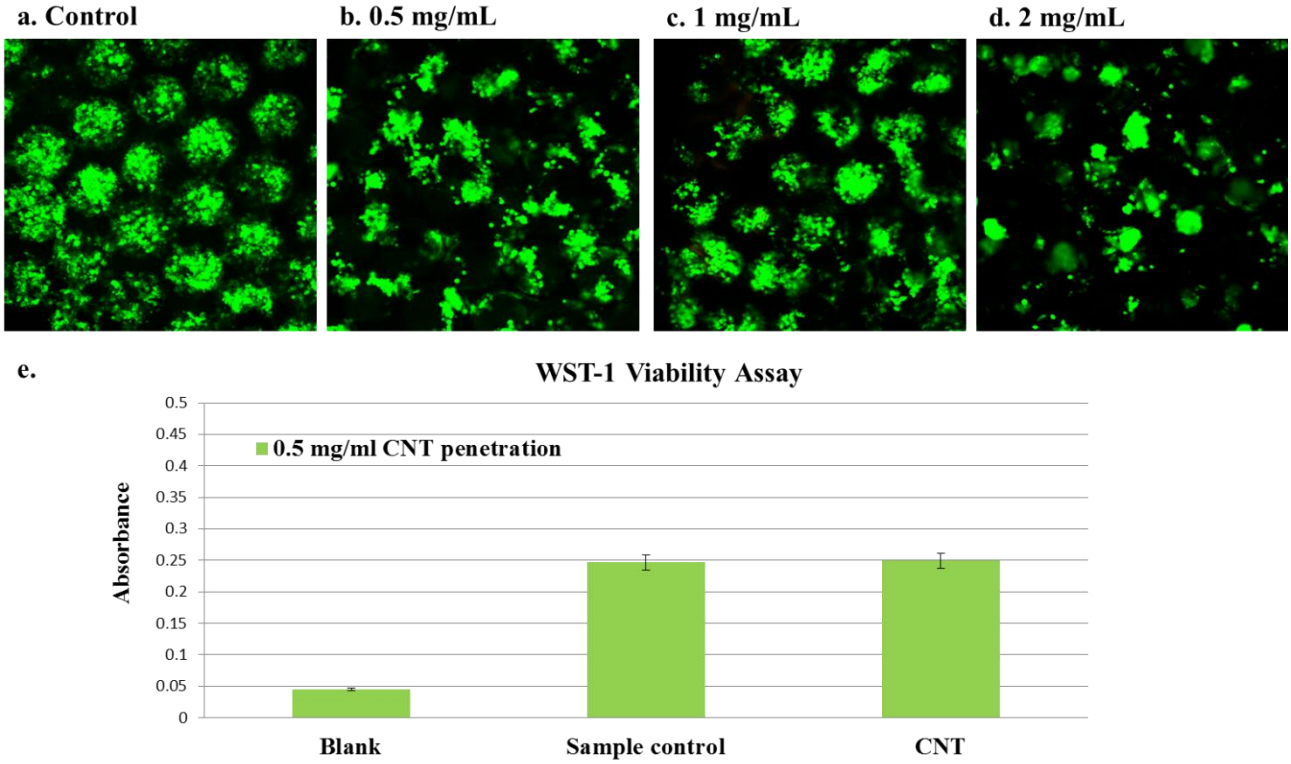

Figure S3. Confocal images of live/dead cell viability assay (LIVE/DEAD Viability/Cytotoxicity Kit, Invitrogen, US) of HepG2 cells in spheroids cultured for 3 days in medium containing (**a**, control) 0, **(b)**, 0.5, (**c**) 1, and (**d**) 2 mg/mL CNTs (P-3, Carbon Solution, Inc.) in the culture medium (Eagle's Minimum Essential Medium (EMEM) supplemented with 10% Fetal Bovine Serum (FBS) and 1% Penicillin–Streptomycin (ATCC)). (**e**) WST-1 assay for HepG2 spheroids cultured with 0.5 mg/mL of CNTs as-prepared (**SI**) for 2 hours. Absorbance values obtained with non-treated groups maintained under identical conditions were taken as 100%. *P < 0.01 compared to control.

Fluorescence Data of Control CNTs. To investigate the possibility of TGFβ1 physically adhered to CNTs nonspecifically. The control experiment was carried out as following. TGFβ1 (5μg, 25kDa) was tagged with TexasRed (Excitation/Emission: 540/620 nm). Tagged TGFβ1 was incubated with 2ml of fluorescent CNTs (CNTs-FITC, 0.5mg/ml) (Excitation/Emission: 460/528 nm) overnight and washed by centrifugal filters (Cutoff Size: 50kDa). Fluorescent intensity of TexasRed and FITC is shown in the charts below. The results show slight passive adsorption of TGFβ1. However, it shall have very limited influence on the results of apparent diffusion coefficients obtained.

TexasRed (Excitation/Emission: 540/620)	**Fluorescent Intensity**
Blank	23.7±0.5
Washing Buffer	36.3±0.5
TGFβ1(100μg/ml)	16712.0±462.0
CNTs	28.3±1.7
CNTs-FITC	99.7±1.7
CNTs-FITC+TGFβ1 before Washing	289.0±0.5
CNTs-FITC+TGFβ1 after Washing	185.0±1.4

FITC (Excitation/Emission: 460/528)	**Fluorescent Intensity**
Blank	29.3±0.5
Washing Buffer	37.0±0
CNTs	31.3±1.7
CNTs-FITC	12128.3±198.2
CNTs-FITC+TGFβ1 before Washing	27865.0±456.6
CNTs-FITC+TGFβ1 after Washing	11545.7±191.2

Biocompatibility of CNTs. Unless contaminated, CNTs are typically considered to be fairly biocompatible.[37] Because toxicity data for 2D vs 3D assays can be substantially different,[38] we decided to initially carry out two standard live/dead cell viability assays which consisted of calcein AM and ethidium homodimer (EthD-1) (Figure S3.a-d) addressing plasma membrane integrity and esterase activity, respectively (Supplementary Information). Both assays showed that the HepG2 cells in spheroids proliferate normally in contact with medium containing as much as 1 mg/mL CNTs. At 2 mg/mL CNT, the viability starts to decrease, which is higher than similar toxicity thresholds reported for CNTs in 2D cultures.[37] Considering these data, we chose the concentration of CNTs of 0.5 mg/mL for permeation studies. Additional test WST-1 assay (Figure S3.e) at this concentration was used to quantify cellular proliferation, viability, and cytotoxicity, based on the reduction of tetrazolium salt to formazan by electron transport across the plasma membrane of dividing cells. It indicated that the viability of CNT-treated cells is identical within the experimental error to HepG2 spheroids in CNT-free media (control).

Confocal Microscopy. Stained with live/dead assay, live cells are green, while dead cells show red. In live/dead assay test, contracted HepG2 spheroids in ICC scaffolds were treated with 0.5 mg/mL, 1mg/mL, and 2 mg/mL CNTs in culture medium for 2 h, with non-treated spheroids used as the control. To be observed by Confocal Microscopy during penetration, HepG2 cells in spheroids grown in scaffolds were pre-labeled by Orange CMTMR (Invitrogen, CA); And CNTs labeled with FITC were added onto scaffolds under the microscope. After 20 min, observation of the penetration process was started through a confocal microscope and 36 images were taken of the whole spheroid by z-stack every 20 min. The process of FITC and Rhodamin B (RhB) molecules penetration into spheroids was observed in the same way as the CNTs.

Quantitative Analysis of Experimental/Effective Diffusion Coefficients based on Confocal Images. Z-stack confocal images including the central panel of spheroids were captured at time points of 20, 40, 60, 80, 100, and 120 min. Here we employed Fick's Second Law[39-43] (1) of diffusion, which relates the flux to the concentration gradients:

$$\frac{\partial C}{\partial t} = D_a \cdot \frac{1}{r^2}\frac{\partial}{\partial r} \cdot \left(r^2 \cdot \frac{\partial C}{\partial r}\right) \qquad \textbf{Eq.S1,}$$

where C = concentration, t = time, r = distance/radius, D_a = diffusion coefficient. We assumed that the diffusing substance moves into the center of the spheroid and the boundary at $r = 0$ is the surface of the spheroid:

(i) $C(0, t) = C_0, t \geq 0$ (L is the mean diameter of 3D tumor tissue model);

(ii) $C(R, t) = 0, t = 0;$

(iii) At $r = d, \partial^2 C/\partial t^2 = 0$ (d is the measure of penetration depth at a certain time point). Then we obtained the equation regarding the depth d and time t from

$$d^2 = 6\pi D_a \cdot t \qquad \textbf{Eq.S2}$$

In our model of diffusion, the tumor tissue-like spheroid is considered as a sphere of radius L. Under the boundary conditions of the experiments performed, this depth of highest concentration in the diffusion front was the measure of penetration depth d. Firstly, according to the z-stack and cross-section images, depth d in equation (2) represents how far fluorescence reached inside the spheroid, where the fluorescence represents FITC, RhB, and CNTs or their derivatives. These data of depth d and time t abstracted from images will be substituted into equation (2) and certain values of D_{ex} will be fit to find the best value of D that minimizes the error by statistically analysis of *Mathematica 8.0*. (Example of z-stack images Figure S4-9 and corresponding *Mathematica* code is shown below)

Figure S4. Z-stack confocal images of CNT-TGFβ1-FITC permeation at 20 min.

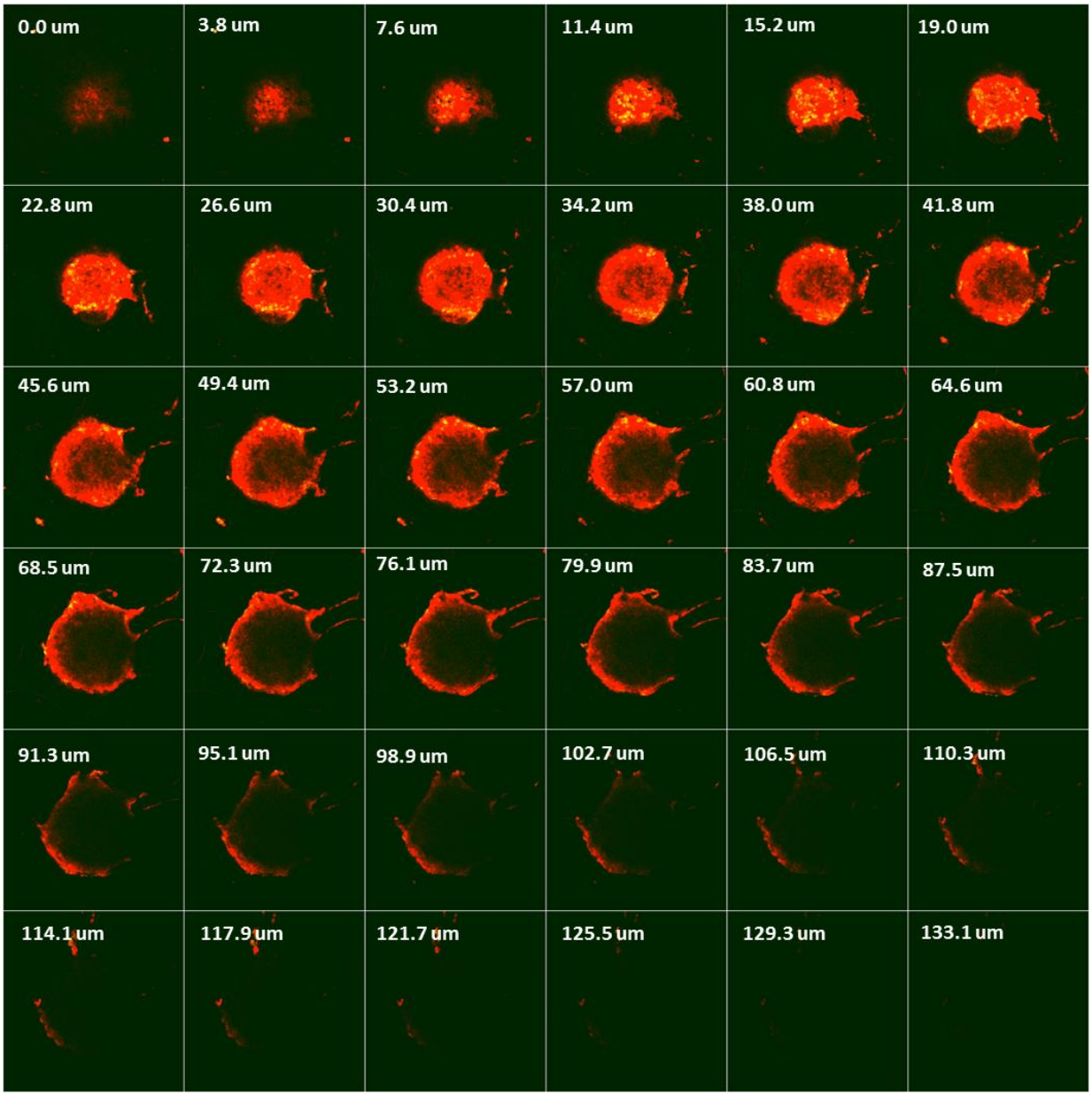

Figure S5. Z-stack confocal images of CNT-TGFβ1-FITC permeation at 40 min.

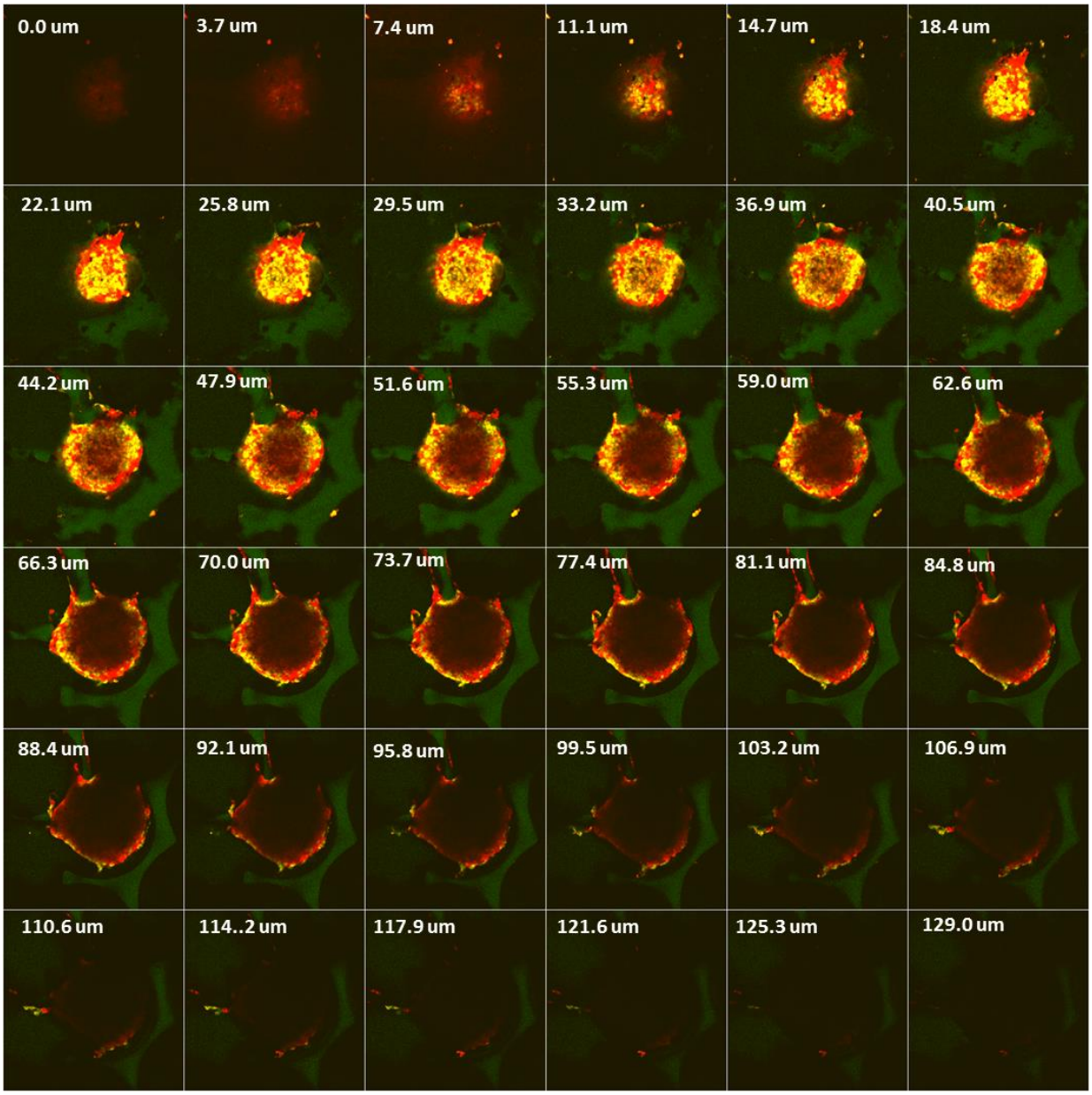

Figure S6. Z-stack confocal images of CNT-TGFβ1-FITC permeation at 60 min.

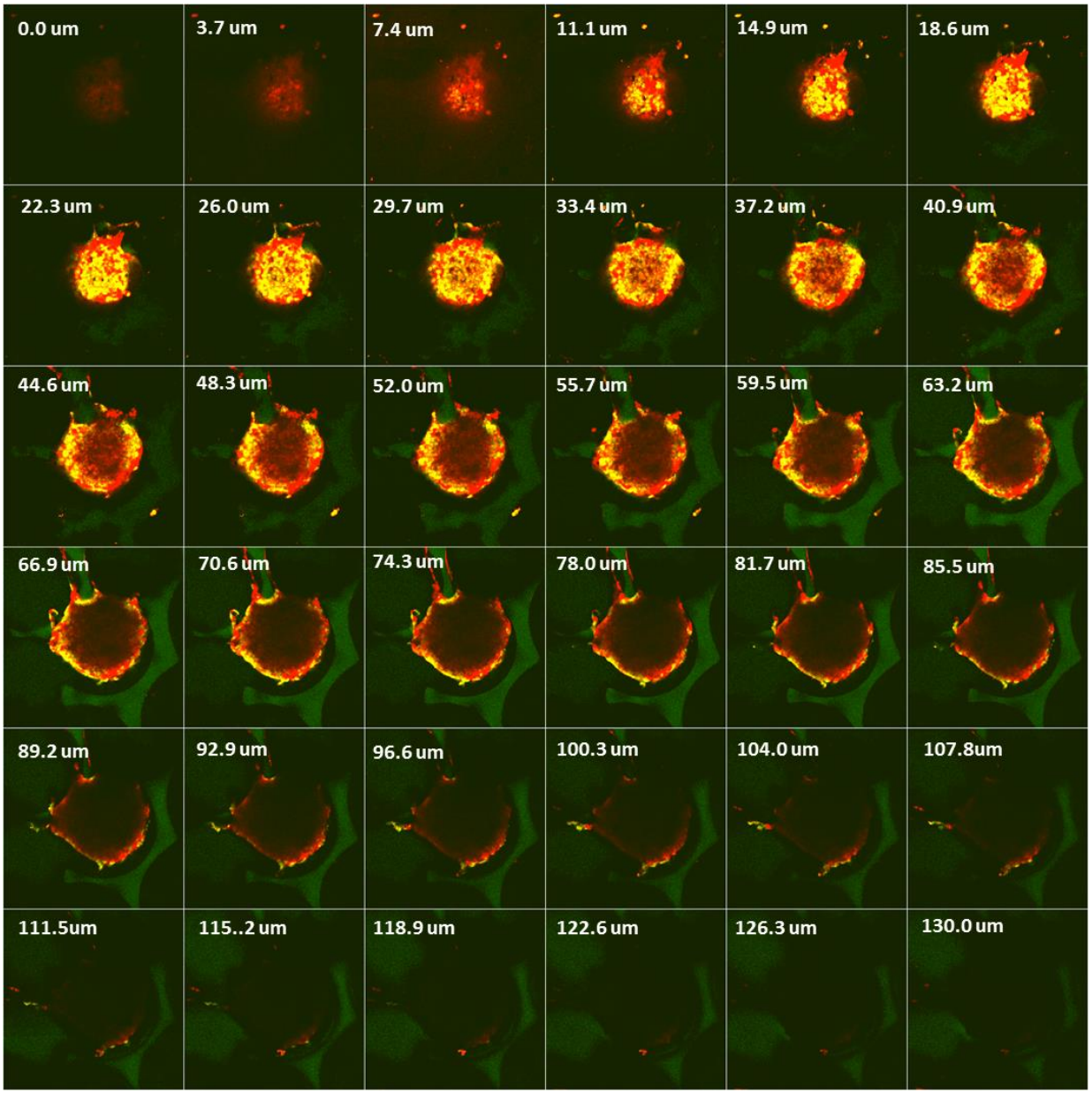

Figure S7. Z-stack confocal images of CNT-TGFβ1-FITC permeation at 80 min.

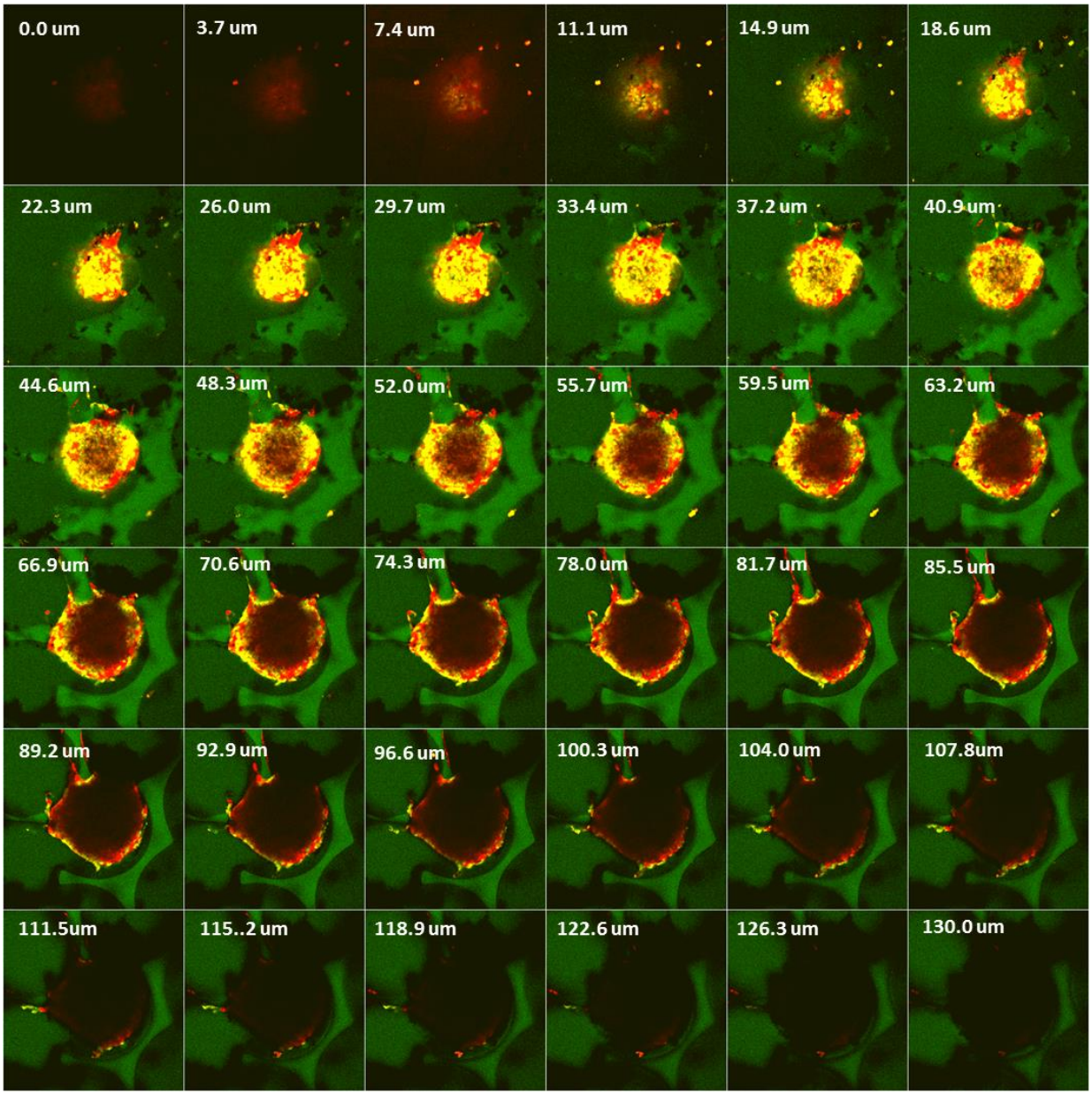

Figure S8. Z-stack confocal images of CNT-TGFβ1-FITC permeation at 100 min.

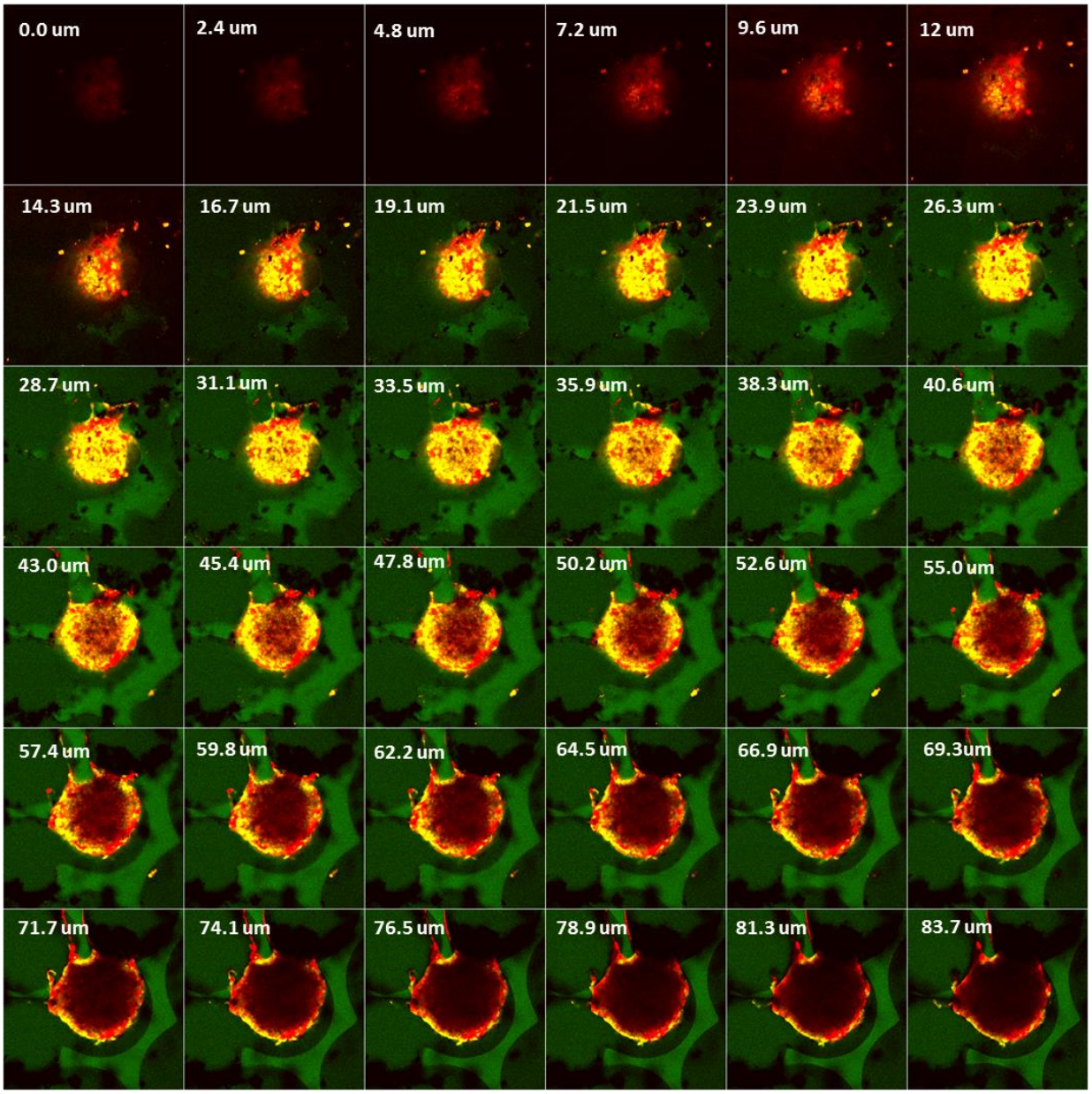

Figure S9. Z-stack confocal images of CNT-TGFβ1-FITC permeation at 120 min.

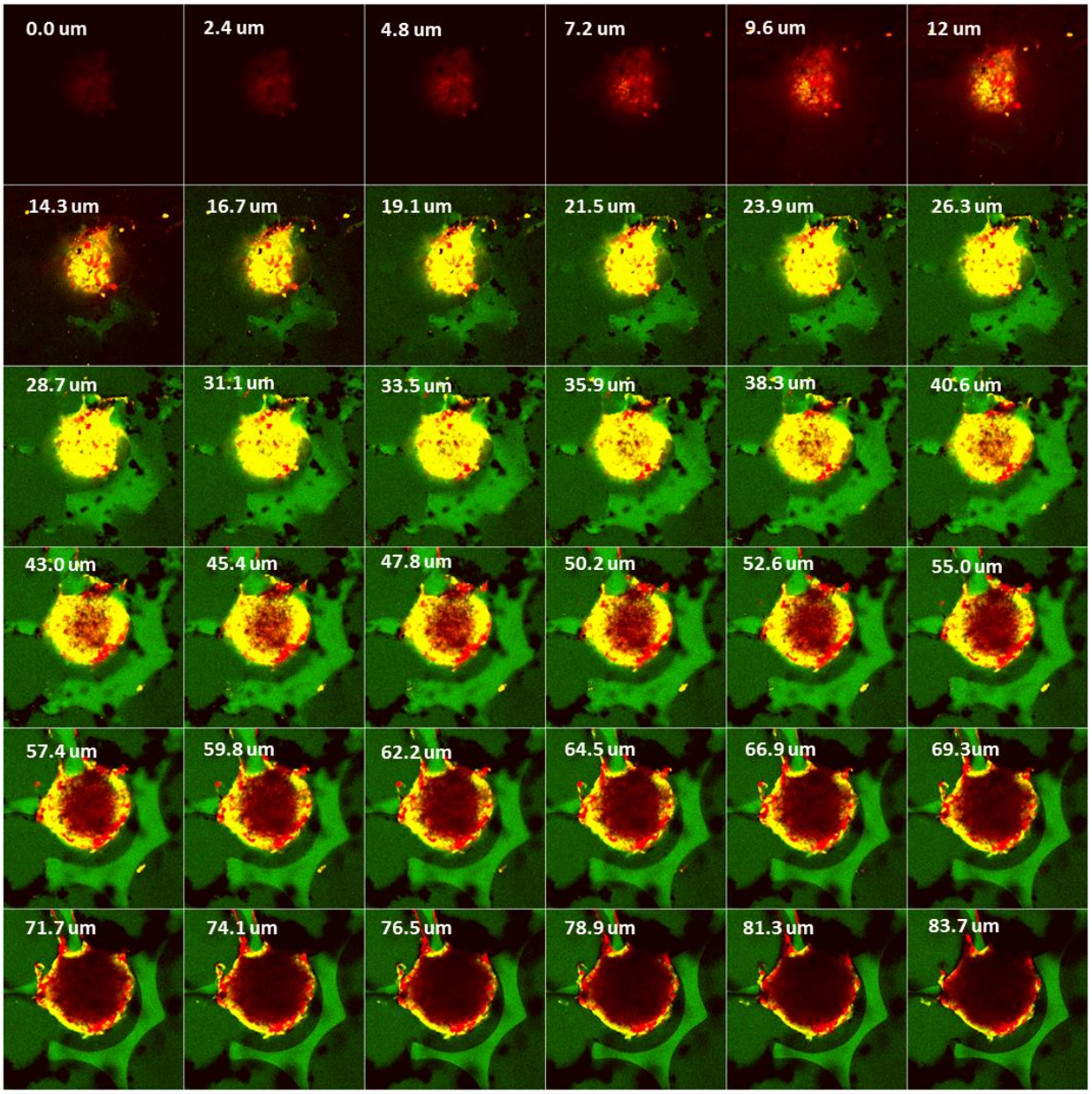

***Mathematica* Code for Data Processing** (Example: one set of data from images in main text**)**

```
c0 = 0.0005 (* Initial concentration *)
0.0005

ct[x_, t_, d_] := c0 * x * (Exp[-x^2 / (4 t * d)]) / (2 * Sqrt[π * t * d])
(* Define concentration function to distance x (m),
time t (s) and diffusion coefficient d based on solutions of
 Equation (1) and derived from one dimensional diffusion solution*)

gradient = D[ct[x, t, d], {{x}}]
    (* Function of gradient *)
```

$$\left\{\frac{0.000141047\, e^{-\frac{x^2}{4dt}}}{\sqrt{d\,t}} - \frac{0.0000705237\, e^{-\frac{x^2}{4dt}}\, x^2}{d\,t\,\sqrt{d\,t}}\right\}$$

```
Dgradient = D[ct[x, t, d], {{x}, 2}][[1]]
 (* Define function of Dgradient to distance, time and diffusion coefficient *)
```

$$\left\{-\frac{0.000211571\, e^{-\frac{x^2}{4dt}}\, x}{d\,t\,\sqrt{d\,t}} + \frac{0.0000352618\, e^{-\frac{x^2}{4dt}}\, x^3}{d^2\,t^2\,\sqrt{d\,t}}\right\}$$

```
Solve [Dgradient == 0, x]
```

$$\left\{\{x \to 0.`\}, \left\{x \to -2.449489742783178` \sqrt{d}\ \sqrt{t}\right\}, \left\{x \to 2.449489742783178` \sqrt{d}\ \sqrt{t}\right\}\right\}$$

```
(*when the gradient change reach the peak,
the equation (2) can be derived from equation (1) *)

t1 = 1200
t2 = 2400
t3 = 3600
t4 = 4800
t5 = 6000
t6 = 7200
 (* time point as seconds "s" *)

x1 = 0.0000114
x2 = 0.0000369
x3 = 0.0000372
x4 = 0.0000409
x5 = 0.0000409
x6 = 0.0000454

(* depth data from images (meter "m") *)
```

```
(({2.44949` Sqrt[d] Sqrt[t] /. t → t1} - x1)^2 + ({2.44949` Sqrt[d] Sqrt[t] /. t → t2} - x2)^2 +
 ({2.44949` Sqrt[d] Sqrt[t] /. t → t3} - x3)^2 + ({2.44949` Sqrt[d] Sqrt[t] /. t → t4} - x4)^2 +
 ({2.44949` Sqrt[d] Sqrt[t] /. t → t5} - x5)^2 + ({2.44949` Sqrt[d] Sqrt[t] /. t → t6} - x6)^2
```

$$\left\{\left(-0.0000114 + 84.8528\sqrt{d}\right)^2 + \left(-0.0000369 + 120.\sqrt{d}\right)^2 + \left(-0.0000372 + 146.969\sqrt{d}\right)^2 + \left(-0.0000409 + 169.706\sqrt{d}\right)^2 + \left(-0.0000409 + 189.737\sqrt{d}\right)^2 + \left(-0.0000454 + 207.846\sqrt{d}\right)^2\right\}$$

```
(*Least square method to fined the best diffusion coefficient*)
```

```
Dvalue = D[{{{(-0.0000114` + 84.85282265263778` Sqrt[d])^2 +
      (-0.0000369` + 120.00001260099934` Sqrt[d])^2 +
      (-0.0000372` + 146.9694` Sqrt[d])^2 + (-0.0000409` + 169.70564530527557` Sqrt[d])^2 +
      (-0.0000409` + 189.73667953403213` Sqrt[d])^2 +
      (-0.0000454` + 207.8461187338364` Sqrt[d])^2}}, {{d}}]
```

$$\left\{\left\{\left\{\frac{84.8528\left(-0.0000114 + 84.8528\sqrt{d}\right)}{\sqrt{d}} + \frac{120.\left(-0.0000369 + 120.\sqrt{d}\right)}{\sqrt{d}} + \frac{146.969\left(-0.0000372 + 146.969\sqrt{d}\right)}{\sqrt{d}} + \frac{169.706\left(-0.0000409 + 169.706\sqrt{d}\right)}{\sqrt{d}} + \frac{189.737\left(-0.0000409 + 189.737\sqrt{d}\right)}{\sqrt{d}} + \frac{207.846\left(-0.0000454 + 207.846\sqrt{d}\right)}{\sqrt{d}}\right\}\right\}\right\}$$

```
Solve[1/Sqrt[d] 84.85282265263778` (-0.0000114` + 84.85282265263778` Sqrt[d]) +
   1/Sqrt[d] 120.00001260099934` (-0.0000369` + 120.00001260099934` Sqrt[d]) +
   146.9694` (-0.0000372` + 146.9694` Sqrt[d])/Sqrt[d] + 1/Sqrt[d]
   169.70564530527557` (-0.0000409` + 169.70564530527557` Sqrt[d]) + 1/Sqrt[d]
   189.73667953403213` (-0.0000409` + 189.73667953403213` Sqrt[d]) + 1/Sqrt[d]
   207.8461187338364` (-0.0000454` + 207.8461187338364` Sqrt[d]) == 0, d]
```

$$\left\{\left\{d \to 5.35836 \times 10^{-14}\right\}\right\}$$

In[155]:=
```
(*Plot the Depth vesus Time*)

Solve[D[ct[x, t, d], {{x}, 2}][[1]][[1]] = 0, {x}]
```

In[156]:= $\{\{x \to 0.`\}, \{x \to -2.449489742783178` \sqrt{d}\ \sqrt{t}\}, \{x \to 2.449489742783178` \sqrt{d}\ \sqrt{t}\}\}$

In[157]:=
```
kk = D[ct[x, t, d], {{x}}][[1]] /. {d → 5.35836206921357`*^-14, t → 1200}
```

Out[157]= $17.5897\, e^{-3.888\times10^{9} x^2} - 1.36778 \times 10^{11}\, e^{-3.888\times10^{9} x^2}\, x^2$

In[159]:=
```
Plot[Sqrt[6 * d * t] /. {d → 5.35836206921357`*^-14}, {t, 0, 7200}]
```

Out[159]=

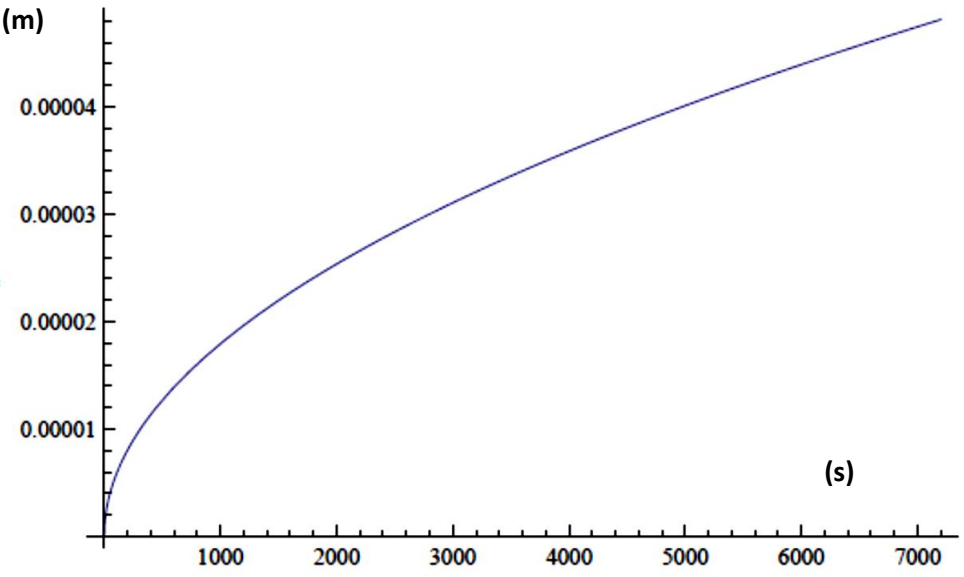

Calculation of Theoretical Diffusion Coefficients of CNTs, FITC, TGFβ1, and RhB. Theoretical diffusion coefficient D_0 for spherical particle related to the temperature T and the friction coefficient f_0 can be calculated using the Stokes equation:

$$D_0 = \frac{k_b T}{f_0} \qquad \text{Eq.S3}$$

$$f_0 = 6\pi\eta L_0 \qquad \text{Eq.S4}$$

where k_b = 1.38 × 10^{-20} $m^2 \cdot g/(s^2 \cdot K)$, T = 293 K, η = viscosity of the solute, L_0 = radius of a spherical particle or molecule with a volume equal to the volume of a rod-like particle or molecule. Frictional coefficient is determined by the viscosity of the media and diameter of the spherical particle.

The frictional coefficient f_n of a non-spherical particle (rod or tube) is usually larger than that of a spherical one of the same volume because there is a larger surface area in contact with the solvent. Therefore, assuming D_n is the theoretical diffusion coefficient for non-spherical particles, when the particle is non-spherical such as a CNT, we could suppose a CNT as a rod-like particle which has a length a = 1000 nm/2 and radius b = 1.55nm/2 (Carbon Solution, Inc. Data sheet.). Its volume is given by the formula:

$$V_{rod} = 2\pi a b^2 \qquad \text{Eq.S5}$$

The aspect ratio P can be defined as: $P = a/b$ = 645.2. The frictional coefficient of a rod-like particle can be calculated as **(6)**

$$f_n = f_0 \frac{(\frac{2}{3})^{1/3} P^{2/3}}{ln(2P) - 0.3} \qquad \text{Eq.S6}$$

Relative diameter L_n of rod-like particle is determined to be 7.67 nm by equation **(7)** [44]

$$L_n = \sqrt[3]{\frac{3ab^2}{2}} \qquad \text{Eq.S7}$$

f_0 is calculated to be 7.52×10^{-4} g/s in tumor tissue (η = 5.2 ± 2.5 Pa·s).[45]

$$f_0 = 6\pi\eta R_0 = 6 \times \pi \times 5.2 \times 10^3 \text{ g/(s·m)} \times 7.67 \text{ m} \times 10^{-9} = 7.52 \times 10^{-4} \text{ g/s}$$

$$D_0 = (1.38 \times 10^{-16} \text{ g·cm}^2/\text{s}^2 \times 293 \text{ K})/7.52 \times 10^{-4} = 5.4 \times 10^{-15} \text{ m}^2/\text{s}$$

Thus f_n equals 9.91×10^{-5} g/s for tumor tissue according to equation (4). Theoretical D_n value of rod-shaped CNTs in tumor tissue is determined to be 5.7×10^{-16} m^2/s.

To calculate the theoretical diffusion coefficients of TGFβ1, FITC, and RhB, it was assumed that these molecules were rod-shaped, where the longest distance in the molecular structure is represented by ***a*** and the shortest by ***b.*** The molecular structure and distance of TGFβ1 between atoms were reported in a previous study[1] (Figure S10.a). Moreover, ***a*** and ***b*** of FITC and Rhodamin were analyzed and measured using software Spartan 10 (Figures S10. b and c). ***P*** will be calculated based on values of ***a*** and ***b*** for each type of molecule. Thereafter, theoretical diffusion coefficients were calculated using the same theory as described above.

1. TGFβ1

$$L_0 = \sqrt[3]{\frac{3ab^2}{2}} = \sqrt[3]{\frac{3 \times 1.607 \times 1.152^2}{2}} = 6.027\ nm$$

$$f_0 = 6\pi\eta L_0 = 6 \times \pi \times 5.2 \times 10^3 \text{ g/(s·m)} \times 6.027 \times 10^{-9} \text{ m} = 5.9 \times 10^{-4} \text{ g/s}$$

$$D_0 = \frac{k_b T}{f_0} = 1.38 \times 10^{-16} \text{ g·cm}^2/\text{s}^2 \times 293 \text{ K} / 5.9 \times 10^{-4} \text{g/s} = 6.9 \times 10^{-15} \text{ m}^2/\text{s}$$

$$f_n = f_0 \frac{(\frac{2}{3})^{1/3} P^{2/3}}{ln(2P) - 0.3} = 5.9 \times 10^{-4} \text{ g/s} \times \frac{(\frac{2}{3})^{1/3} 2.724^{2/3}}{ln(2 \times 2.724) - 0.3} = 7.1 \times 10^{-4} \text{ g/s}$$

$\boldsymbol{D_n} = \frac{\boldsymbol{k_b T}}{\boldsymbol{f_n}}$ = 1.38 × 10^{-16} g·cm^2/s^2 × 293 K /7.1 × 10^{-4} g/s = 5.7 × 10^{-15} m^2/s

2. FITC

$$\boldsymbol{L_0} = \sqrt[3]{\frac{\boldsymbol{3ab^2}}{\boldsymbol{2}}} = \sqrt[3]{\frac{3 \times 0.945 \times 0.4634^2}{2}} = 0.673 \text{ nm}$$

$\boldsymbol{f_0} = \boldsymbol{6\pi\eta L_0}$ = 6 × $\boldsymbol{\pi}$ × 5.2 × 10^3 g/(s·m) × 0.673 × 10^{-9} m = 6.6 × 10^{-5} g/s

$\boldsymbol{D_0} = \frac{\boldsymbol{k_b T}}{\boldsymbol{f_0}}$ =1.38 × 10^{-16} g·cm^2/s^2 K^{-1} × 293 K /6.6 × 10^{-5} g/s = 6.1 × 10^{-14} m^2/s

$\boldsymbol{f_n} = \boldsymbol{f_0}\ \frac{(\frac{2}{3})^{1/3}\boldsymbol{P^{2/3}}}{\boldsymbol{ln(2P)-0.3}}$ = 6.6 × 10^{-5} g/s × $\frac{(\frac{2}{3})^{1/3}\boldsymbol{1.395^{2/3}}}{\boldsymbol{ln(2\times 1.395)-0.3}}$ = 9.91 × 10^{-5} g/s

$\boldsymbol{D_n} = \frac{\boldsymbol{k_b T}}{\boldsymbol{f_n}}$ = 1.38 × 10^{-20} g·m^2/s^2 K^{-1} × 293K /9.91 × 10^{-5} g/s = 4.1 × 10^{-14} m^2/s

3. RhB

$$\boldsymbol{L_0} = \sqrt[3]{\frac{\boldsymbol{3ab^2}}{\boldsymbol{2}}} = \sqrt[3]{\frac{3 \times 1.607 \times 1.152^2}{2}} = 1.473\ nm$$

$\boldsymbol{f_0} = \boldsymbol{6\pi\eta L_0}$ = 6 × $\boldsymbol{\pi}$ × 5.2 × 10^3 g/(s·m) × 1.473 m 10^{-9} = 1.45×10^{-4} g/s

$\boldsymbol{D_0} = \frac{\boldsymbol{k_b T}}{\boldsymbol{f_0}}$ =1.38 × 10^{-16} g·cm^2/s^2 K^{-1} × 293K /1.45 × 10^{-4} g/s = 2.8 × 10^{-14} m^2/s

$\boldsymbol{f_n} = \boldsymbol{f_0}\ \frac{(\frac{2}{3})^{1/3}\boldsymbol{P^{2/3}}}{\boldsymbol{ln(2P)-0.3}}$ = 1.45 × 10^{-4} g/s × $\frac{(\frac{2}{3})^{1/3}\boldsymbol{1.395^{2/3}}}{\boldsymbol{ln(2\times 1.395)-0.3}}$ = 2.2 × 10^{-4} g/s

$\boldsymbol{D_n} = \frac{\boldsymbol{k_b T}}{\boldsymbol{f_n}}$ = 1.38 × 10^{-16} g·cm^2/s^2 K^{-1} × 293K /2.2 × 10^{-4} g/s = 1.8 × 10^{-14} m^2/s

$\boldsymbol{D_0}$ is the diffusion coefficient for a spherical shape ; $\boldsymbol{D_n}$ is the diffusion coefficient for a rod shape. The values of theoretical diffusion coefficients in tissue were shown in **Table 1.**

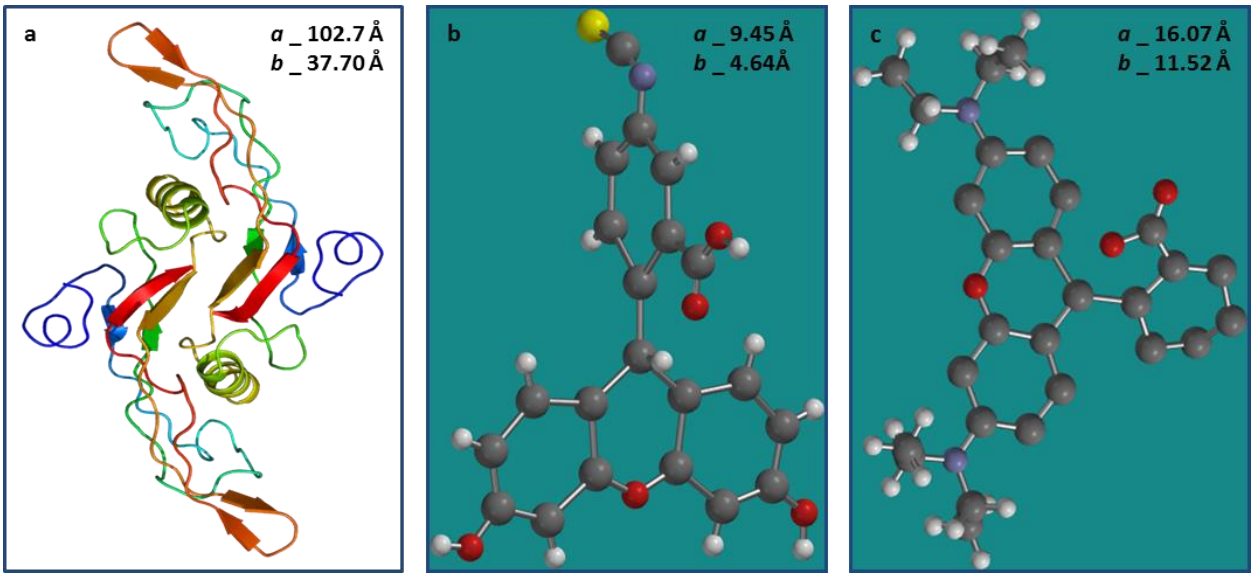

Figure S10. The molecular structure and distance of TGFβ1[1] (**a**), FITC (**b**) and RhB (**c**) where ***a*** is the longest distance between atoms in one structure, and ***b*** is the radius of stimulated molecular structure. Spheres (atoms) of (**b**) and (**c**): Grey-C; White-H; Red-O; Purple-N; Yellow-S.

Cell-CNTs Interaction *in vitro*. Previous studies showed that surface properties of CNTs have an effect on cell internalization and excretion of nanoparticles and molecules.[46] To determine how the different surfaces of CNTs influenced their interactions with cell membranes in our case, we first blocked the energy-enabled membrane transport of cells for the CNTs and their derivatives with FITC at 4 °C and 37 °C by treating the cells with sodium azide and 2-deoxyglucose. Subsequently, we carried out confocal fluorescence microscopy studies of their uptake and intracellular distribution in living cells without endocytosis (Figure S11). By analysis of confocal images, it was found that without endocytosis, CNTs and their derivatives can both penetrate into cells by direct insertion. When the temperature decreased, the lipid membrane become rigid and reduced the penetration amount of CNTs. Moreover, fewer CNTs with ligands penetrated into cells through transient pores than regular ones. With blockage of an energy source and thus the endocytosis, the internalization of CNTs is theoretically through lipid-membrane fusion only[47]. The results shows internalization of CNT-TGFβ1-FITC were lower than that of CNT-FITC. Meanwhile, the ratio of endocytosis at normal status was measured by staining and counting endosomes in cells. The images (Figure S12**)** implicated CNT with targeting ligand were internalized more by endocytosis whereas CNT-FITC interacted with cells by a lipid-assisted mechanism for passive insertion without energy supplement. This is potentially due to the shapes of CNTs; that CNTs as elongated tubes are able to penetrate through the plasma membrane with lipid-membrane fusion, as a 'nanosyringe',[47] which is dependent on their hydrophobicity and stability (Figure S13) culture media.[48] This property of nanosyringe possibly hindered CNTs moving forward by free diffusion.

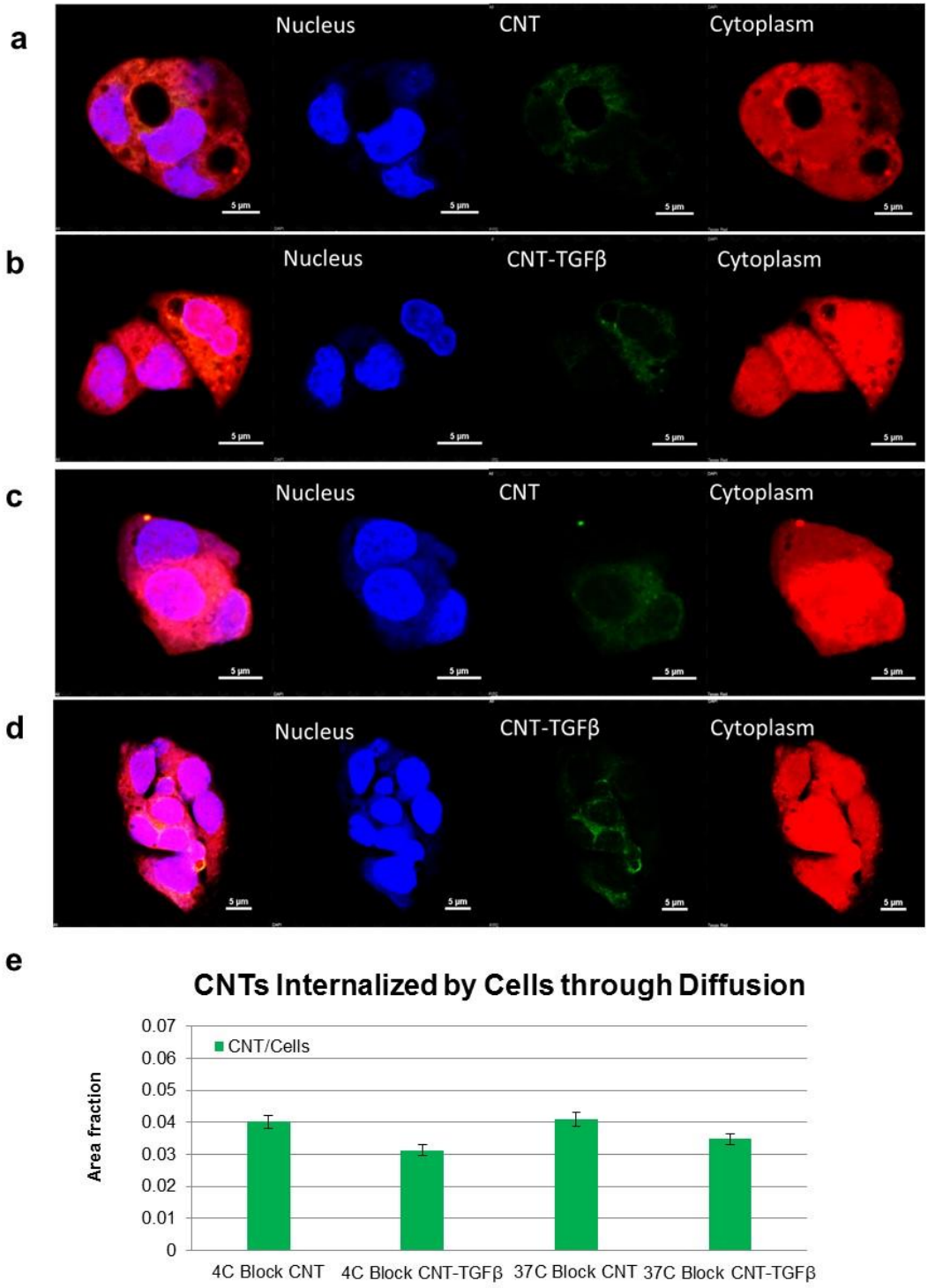

Figure S11. CNTs-FITC and their derivatives CNTs-TGFβ1-FITC entering cells at 4 °C and 37 °C under conditions where active internalization processes are blocked in the presence of azide and 2-deoxyglucose. HepG2 cells were incubated for 20 min in serum-free medium with CNTs-FITC (**a**) or CNTs-TGFβ1-FITC (**b**) at 4 °C and with CNTs-FITC (**c**) or CNTs-TGFβ1-FITC (**d**) at 37 °C. Area fraction of CNTs and their derivatives were calculated (**e**). Nuclei were stained with DAPI (blue) while the cytoplasm was stained with CellTracker™ CMRA (orange-red). Scale bars: 5 μm.

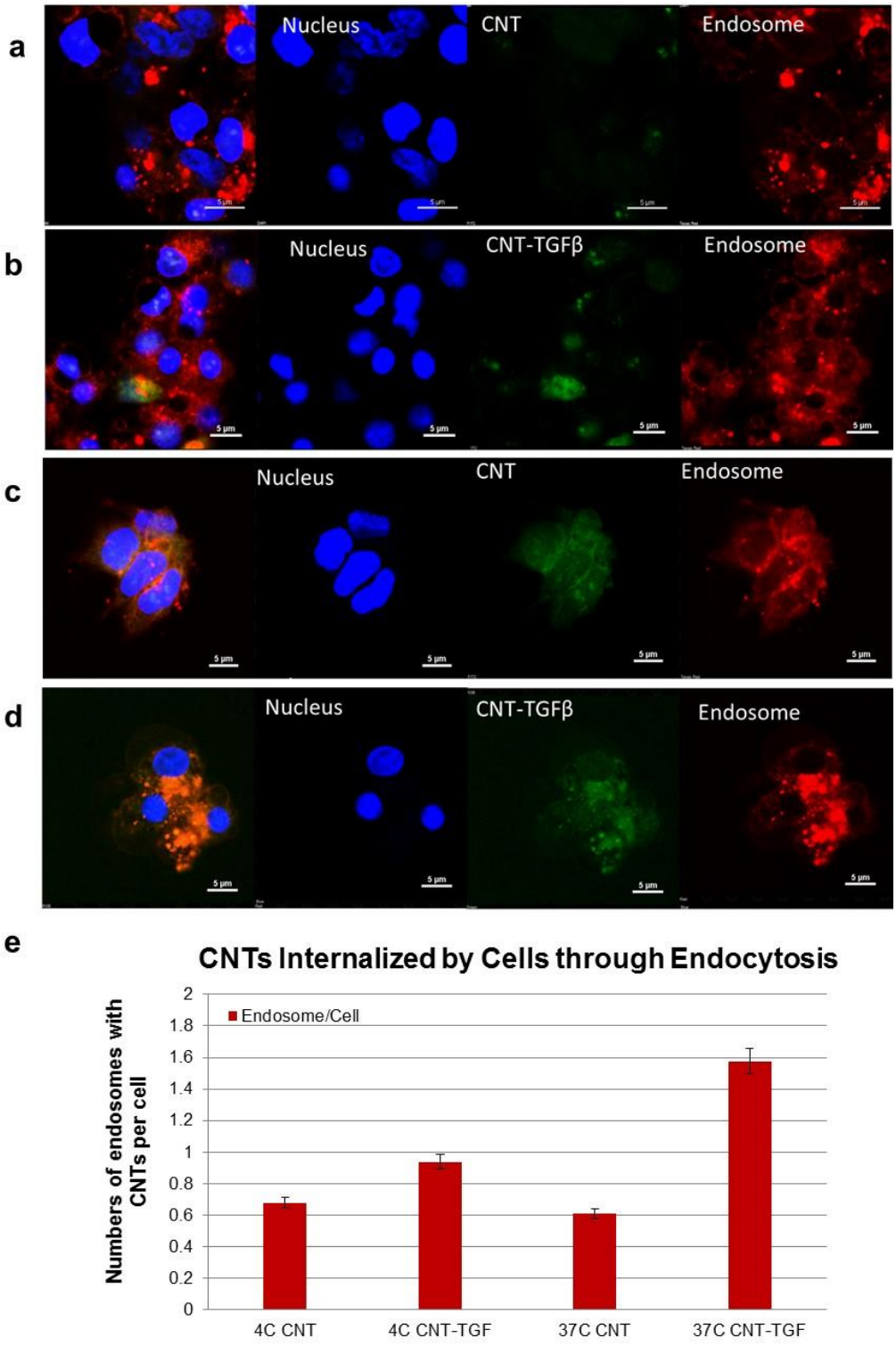

Figure S12. Quantification of CNTs-FITC and their derivatives CNTs-TGFβ1-FITC entering cells by endocytosis at 4 °C and 37 °C. HepG2 cells were incubated for 20 min in serum-free medium with CNTs-FITC (**a**) or CNTs-TGFβ1-FITC (**b**) at 4 °C and with CNTs-FITC (**c**) or CNTs-TGFβ1-FITC (**d**) at 37 °C. Nuclei were counterstained with DAPI (blue) and early endosomes are marked with early Endosomes-RFP. Endosomes were counted and shown in (**e**). Scale bars: 5 μm.

Calculation of apparent diffusion coefficient D_a of CNT-TGFβ1-FITC. Consider interstitial space and interface with the cellular membrane as extracellular space, we can apply the concept of Monte-Carlo tracer method for two-phase transport in porous materials[49] to define D_a.

Based on assumptions of association-dissociation equilibrium (C_{bi} /C_{ex} = K) [50]

$$J = J_{ex} + J_{mem} = -\left[D_{e,ex} + a_v D_{e,mem}\frac{C_{bi}}{C_{ex}}\right]\frac{d\,C_{ex}}{dr'} \qquad \text{Eq. S8}$$

where J_i is the interstitial phase diffusive flux, J_{mem} is the cell membrane surface diffusive flux, $D_{e,i}$ is the effective interstitial phase diffusivity, $D_{e,mem}$ is the effective cell membrane surface diffusivity (length^2/time); C_{ex} is the extracellular concentration, C_{bi} is the cell membrane surface concentration. a_v is volume ratio (cylinder layer-cell membrane to capillary-interstitial layer). r' is the direction of net motion.

For combined interstitial and cell membrane surface diffusion, an effective diffusivity can be described in terms of the diffusivities associated with an equivalent capillary and of tortuosity factors τ for the void and surface phases:

$$D_a = \frac{D_{ex}\,\phi}{\tau_i} + \frac{D_{mem}}{\tau_{mem}}\,a_v K \qquad \text{Eq. S9}$$

D_i and D_{mem} are interstitial phase diffusivity and cell membrane surface diffusivity, in equivalent capillaries. The terms τ_i and τ_{mem} denote the void and surface tortuosities, defined as the length of the equivalent capillary required in order to describe effective diffusivities in the void and surface phases, respectively. ϕ is void fraction of tumor.

$a_v = 2\pi$ (interstitial space size) (cell membrane thickness)×L/π(interstitial space size)^2×L

=2(cell membrane thickness)/(interstitial space diameter) = 2× 8 nm/1343 nm = 0.012[51, 52]

$\boldsymbol{D_{ex}}$ = (1.45±0.65) ×10^{-14} m^2/s in lymph [53]

$\boldsymbol{D_{mem}}$ = (2.3±0.7) ×10^{-12} m^2/s [54]

$\boldsymbol{D_a}$ were shown in **Table 1** of maintext

$\boldsymbol{\phi}$ = 40%~80% (average: 60%) [55]

$\boldsymbol{\tau_{ex} = \tau_{mem} = \frac{L}{C} = \frac{2d}{\pi d} = \frac{2}{\pi}}$ = 0.6 (assume heptocytes are spherical, $\boldsymbol{d}$ is the average radius)

Therefore, if consider the membrane diffusion as part of extracellular diffusion, we have

$\boldsymbol{K = (D_a - \frac{D_{ex}\,\phi}{\tau_{ex}})/(\frac{D_{mem}}{\tau_{mem}}\,a_v)}$

$\boldsymbol{K > 0}$

For **CNT-FITC,**

$\boldsymbol{K_{CNT\text{-}FITC}}$ = ((0.9±0.3) ×10^{-14} m^2/s – 60% × (1.45±0.65) ×10^{-14} m^2/s /0.6)/ ((2.3±0.7)×10^{-12} m^2/s /0.6 × 0.012) ≈ 0 (Range of 0~0.125)

For **CNT -TGFβ1-FITC,**

$\boldsymbol{K_{CNT\text{-}TGF\beta1\text{-}FITC}}$ = ((1.5±0.2) ×10^{-13} m^2/s – 60% × (1.45±0.65) ×10^{-14} m^2/s /0.6)/ ((2.3±0.7) ×10^{-12} m^2/s /0.6 × 0.012) ≈2.95 (Range of 1.81~5.06)

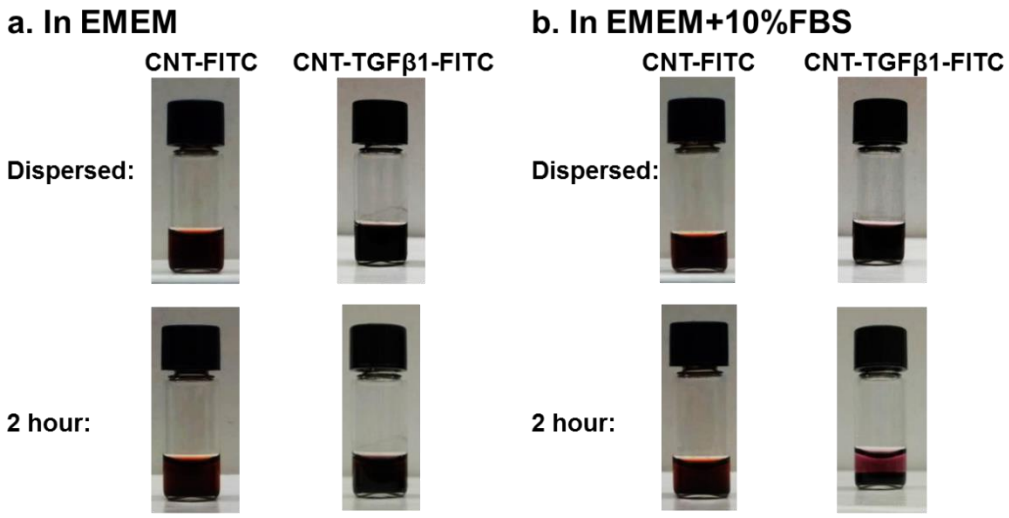

Figure S13. Stability of CNT-FITC and CNT-TGFβ1-FITC in EMEM without (a) and with (b) FBS after 2 hours.

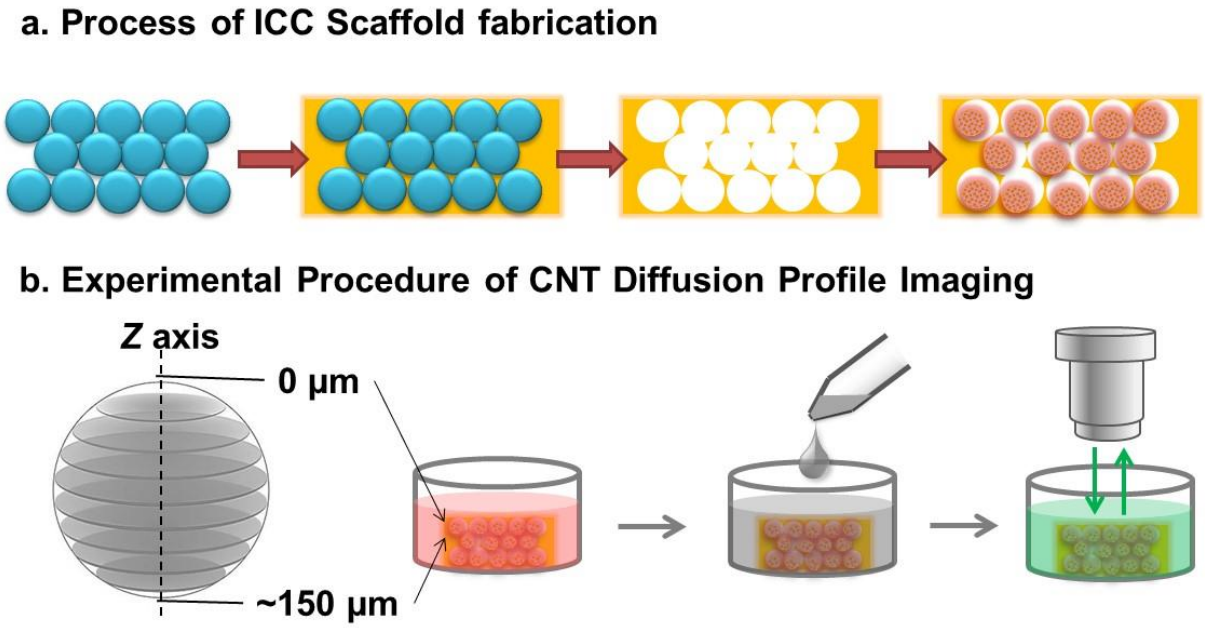

Figure S14. Schematic diagram of ICC scaffold fabrication, cellular spheroid culture and imaging process of CNT diffusion.

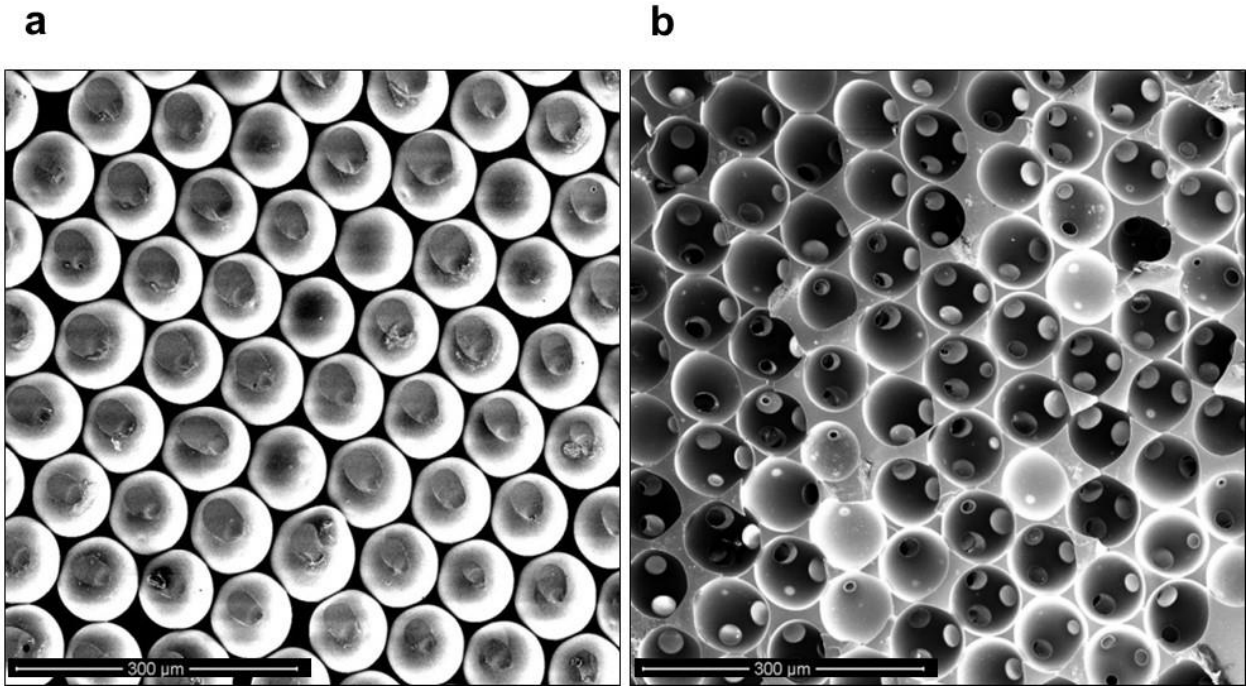

Figure S15. SEM images of dehydrated hydrogel ICC scaffolds **(b)** created by dissolving beads template **(a)** from hydrogel matrix. Pore diameter was shrunk during the dehydration process of SEM preparation. Scale bars: 300µm (**a**) and (**b**).

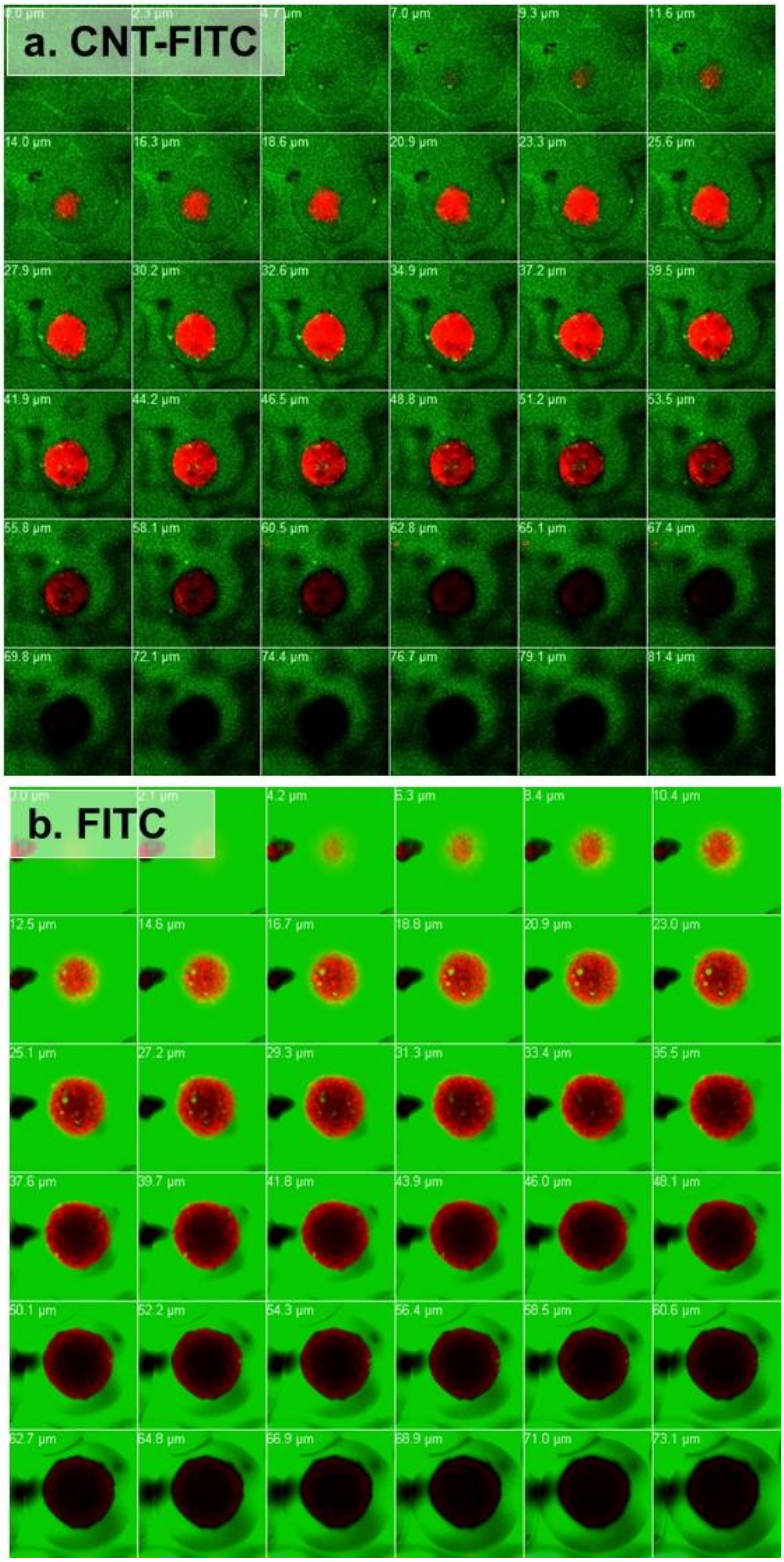

Figure S16. Sliced confocal images of HepG2 spheroids after 20 min exposure **(a)** CNT-FITC and **(b)** FITC (8.7×10^{-5} mg/ml). HepG2 cells in spheroids were stained red (CMTPX) before spheroid formation for images. CNT-FITC and FITC have green fluorescence.

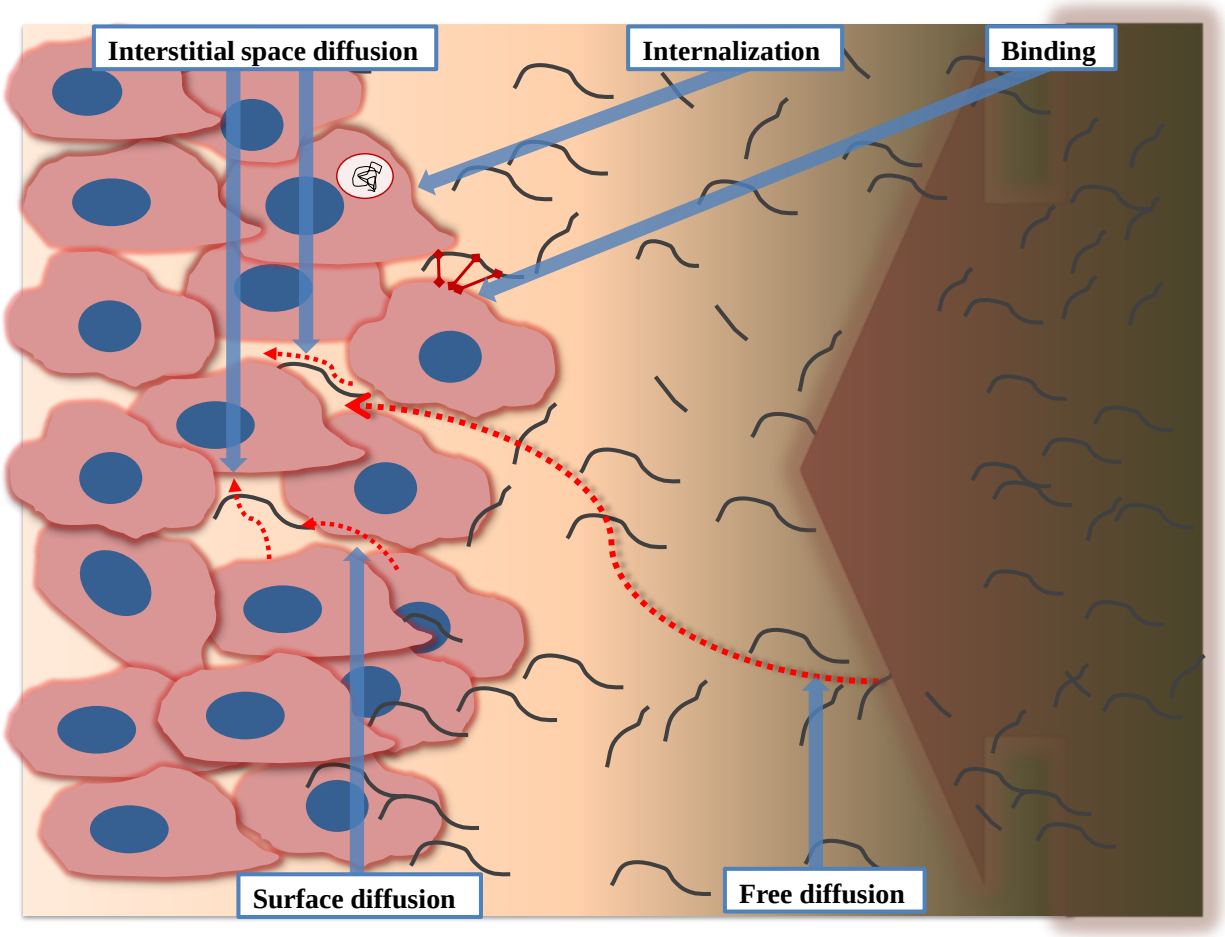

Scheme S1. Transport mechanisms governing CNT penetration through tissues.

REFERENCE

1. Radaev, S.; Zou, Z.; Huang, T.; Lafer, E.M.; Hinck, A.P. & Sun, P.D. Ternary Complex of Transforming Growth Factor-Beta1 Reveals Isoform-Specific Ligand Recognition and Receptor Recruitment in the Superfamily. *J. Biol. Chem.* **2010**, 285,14806-14814.
2. Sanna, V. & Sechi, M. Nanoparticle Therapeutics for Prostate Cancer Treatment. *Nanomedicine* **2012**, 8 Suppl 1,S31-36.
3. Grobmyer, S.R.; Zhou, G.; Gutwein, L.G.; Iwakuma, N.; Sharma, P. & Hochwald, S.N. Nanoparticle Delivery for Metastatic Breast Cancer. *Nanomedicine* **2012**, 8 Suppl 1,S21-30.
4. Egusquiaguirre, S.P.; Igartua, M.; Hernandez, R.M. & Pedraz, J.L. Nanoparticle Delivery Systems for Cancer Therapy: Advances in Clinical and Preclinical Research. *Clin. Transl. Oncol.* **2012**, 14,83-93.
5. Galvin, P.; Thompson, D.; Ryan, K.B.; McCarthy, A.; Moore, A.C.; Burke, C.S.; Dyson, M.; Maccraith, B.D.; Gun'ko, Y.K.; Byrne, M.T.; Volkov, Y.; Keely, C.; Keehan, E.; Howe, M.; Duffy, C. & MacLoughlin, R. Nanoparticle-Based Drug Delivery: Case Studies for Cancer and Cardiovascular Applications. *Cell. Mol. Life. Sci.* **2012**, 69,389-404.
6. Wang, A.Z.; Langer, R. & Farokhzad, O.C. Nanoparticle Delivery of Cancer Drugs. *Annu. Rev. Med.* **2012**, 63,185-198.
7. Perfezou, M.; Turner, A. & Merkoci, A. Cancer Detection Using Nanoparticle-Based Sensors. *Chem. Soc. Rev.* **2012**, 41,2606-2622.
8. Islam, T. & Harisinghani, M.G. Overview of Nanoparticle Use in Cancer Imaging. *Cancer Biomarkers* **2009**, 5,61-67.
9. Davis, M.E.; Chen, Z.G. & Shin, D.M. Nanoparticle Therapeutics: An Emerging Treatment Modality for Cancer. *Nat. Rev. Drug Discovery* **2008**, 7,771-782.
10. Sawicki, J.A.; Anderson, D.G. & Langer, R. Nanoparticle Delivery of Suicide DNA for Epithelial Ovarian Cancer Therapy. *Adv. Exp. Med. Biol.* **2008**, 622,209-219.
11. Brannon-Peppas, L. & Blanchette, J.O. Nanoparticle and Targeted Systems for Cancer Therapy. *Adv. Drug Delivery Rev.* **2004**, 56,1649-1659.
12. Minchinton, A.I. & Tannock, I.F. Drug Penetration in Solid Tumours. *Nat. Rev. Cancer* **2006**, 6,583-592.
13. Lankelma, J.; Dekker, H.; Luque, F.R.; Luykx, S.; Hoekman, K.; van der Valk, P.; van Diest, P.J. & Pinedo, H.M. Doxorubicin Gradients in Human Breast Cancer. *Clin. Cancer Res.* **1999**, 5,1703-1707.
14. Kyle, A.H.; Huxham, L.A.; Yeoman, D.M. & Minchinton, A.I. Limited Tissue Penetration of Taxanes: A Mechanism for Resistance in Solid Tumors. *Clin. Cancer Res.* **2007**, 13,2804-2810.
15. Kuh, H.J.; Jang, S.H.; Wientjes, M.G.; Weaver, J.R. & Au, J.L. Determinants of Paclitaxel Penetration and Accumulation in Human Solid Tumor. *J. Pharmacol. Exp. Ther.* **1999**, 290,871-880.
16. Primeau, A.J.; Rendon, A.; Hedley, D.; Lilge, L. & Tannock, I.F. The Distribution of the Anticancer Drug Doxorubicin in Relation to Blood Vessels in Solid Tumors. *Clin. Cancer Res.* **2005**, 11,8782-8788.
17. Koceva-Chyla, A.; Jedrzejczak, M.; Skierski, J.; Kania, K. & Jozwiak, Z. Mechanisms of Induction of Apoptosis by Anthraquinone Anticancer Drugs Aclarubicin and Mitoxantrone in Comparison with Doxorubicin: Relation to Drug Cytotoxicity and Caspase-3 Activation. *Apoptosis* **2005**, 10,1497-1514.
18. Lin, R.; Shi Ng, L. & Wang, C.H. *In Vitro* Study of Anticancer Drug Doxorubicin in Plga-Based Microparticles. *Biomaterials* **2005**, 26,4476-4485.

19. Chen, Y.; Burton, M.A.; Codde, J.P.; Napoli, S.; Martins, I.J. & Gray, B.N. Evaluation of Ion-Exchange Microspheres as Carriers for the Anticancer Drug Doxorubicin: In-Vitro Studies. *J. Pharm. Pharmacol.* **1992**, 44,211-215.
20. Doxorubicin (Adriamycin)--a New Anticancer Drug. *Med. Lett. Drugs Ther.* **1975**, 17,42-43.
21. Sinha, R.; Vidyarthi, A.S. & Shankaracharya A Molecular Docking Study of Anticancer Drug Paclitaxel and Its Analogues. *Indian J. Biochem. Biophys.* **2011**, 48,101-105.
22. Marsh, R.E.; Tuszynski, J.A.; Sawyer, M. & Vos, K.J. A Model of Competing Saturable Kinetic Processes with Application to the Pharmacokinetics of the Anticancer Drug Paclitaxel. *Math. Biosci. Eng.* **2011**, 8,325-354.
23. Basse, B.; Baguley, B.C.; Marshall, E.S.; Joseph, W.R.; van Brunt, B.; Wake, G. & Wall, D.J. Modelling Cell Death in Human Tumour Cell Lines Exposed to the Anticancer Drug Paclitaxel. *J. Math. Biol.* **2004**, 49,329-357.
24. Long, H.J. Paclitaxel (Taxol): A Novel Anticancer Chemotherapeutic Drug. *Mayo Clin. Proc.* **1994**, 69,341-345.
25. Datta, A.K.; Rakesh, V. & Knovel (Firm) An Introduction to Modeling of Transport Processes : Applications to Biomedical Systems. C.U.P. 2010.
26. Pluen, A.; Boucher, Y.; Ramanujan, S.; McKee, T.D.; Gohongi, T.; di Tomaso, E.; Brown, E.B.; Izumi, Y.; Campbell, R.B.; Berk, D.A. & Jain, R.K. Role of Tumor-Host Interactions in Interstitial Diffusion of Macromolecules: Cranial vs. Subcutaneous Tumors. **2001**, 98,4628-4633.
27. Nugent, L.J. & Jain, R.K. Extravascular Diffusion in Normal and Neoplastic Tissues. *Cancer Res.* **1984**, 44,238-244.
28. Wong, C.; Stylianopoulos, T.; Cui, J.; Martin, J.; Chauhan, V.P.; Jiang, W.; Popovic, Z.; Jain *Proc. Natl. Acad. Sci. U. S. A.*, R.K.; Bawendi, M.G. & Fukumura, D. Multistage Nanoparticle Delivery System for Deep Penetration into Tumor Tissue. *Proc. Natl. Acad. Sci. U. S.A.* **2011**, 108,2426-2431.
29. Chauhan, V.P.; Stylianopoulos, T.; Boucher, Y. & Jain, R.K. Delivery of Molecular and Nanoscale Medicine to Tumors: Transport Barriers and Strategies. *Annu. Rev. Chem. Biomol. Eng.* **2011**, 2,281-298.
30. Geng, Y.; Dalhaimer, P.; Cai, S.; Tsai, R.; Tewari, M.; Minko, T. & Discher, D.E. Shape Effects of Filaments Versus Spherical Particles in Flow and Drug Delivery. *Nat. Nanotechnol.* **2007**, 2,249-255.
31. Chauhan, V.P.; Popovic, Z.; Chen, O.; Cui, J.; Fukumura, D.; Bawendi, M.G. & Jain, R.K. Fluorescent Nanorods and Nanospheres for Real-Time *in Vivo* Probing of Nanoparticle Shape-Dependent Tumor Penetration. *Angew. Chem., Int. Ed. Engl.* **2011**, 50,11417-11420.
32. Ruggiero, A.; Villa, C.H.; Bander, E.; Rey, D.A.; Bergkvist, M.; Batt, C.A.; Manova-Todorova, K.; Deen, W.M.; Scheinberg, D.A. & McDevitt, M.R. Paradoxical Glomerular Filtration of Carbon Nanotubes. *Proc. Natl. Acad. Sci. U. S. A.* **2010**, 107,12369-12374.
33. Yoo, J.W.; Doshi, N. & Mitragotri, S. Adaptive Micro and Nanoparticles: Temporal Control over Carrier Properties to Facilitate Drug Delivery. *Adv. Drug Delivery Rev.* **2011**, 63,1247-1256.
34. Franzen, S. & Lommel, S.A. Targeting Cancer with 'Smart Bombs': Equipping Plant Virus Nanoparticles for a 'Seek and Destroy' Mission. *Nanomedicine* **2009**, 4,575-588.
35. Gert Storm, S.O.B., Toos Daemen, Danilo D. Lasic Surface Modification of Nanoparticles to Oppose Uptake by the Mononuclear Phagocyte System. *Adv. Drug Delivery Rev.* **1995**, 17,31-48.
36. Campbell, R.B.; Fukumura, D.; Brown, E.B.; Mazzola, L.M.; Izumi, Y.; Jain, R.K.; Torchilin, V.P. & Munn, L.L. Cationic Charge Determines the Distribution of Liposomes between the Vascular and Extravascular Compartments of Tumors. *Cancer Res.* **2002**, 62,6831-6836.

37. Ren, H.X.; Chen, X.; Liu, J.H.; Gu, N. & Huang, X.J. Toxicity of Single-Walled Carbon Nanotube: How We Were Wrong? *Mater. Today* **2010**, 13,6-8.
38. Lee, J.; Lilly, G.D.; Doty, R.C.; Podsiadlo, P. & Kotov, N.A. *In Vitro* Toxicity Testing of Nanoparticles in 3d Cell Culture. *Small* **2009**, 5,1213-1221.
39. Egusquiaguirre, S.P.; Igartua, M.; Hernandez, R.M. & Pedraz, J.L. Nanoparticle Delivery Systems for Cancer Therapy: Advances in Clinical and Preclinical Research. *Clin. Transl. Oncol.* **2012**, 14,83-93.
40. Pridgen, E.M.; Langer, R. & Farokhzad, O.C. Biodegradable, Polymeric Nanoparticle Delivery Systems for Cancer Therapy. *Nanomedicine* **2007**, 2,669-680.
41. Galvin, P.; Thompson, D.; Ryan, K.B.; McCarthy, A.; Moore, A.C.; Burke, C.S.; Dyson, M.; MacCraith, B.D.; Gun'ko, Y.K.; Byrne, M.T.; Volkov, Y.; Keely, C.; Keehan, E.; Howe, M.; Duffy, C. & MacLoughlin, R. Nanoparticle-Based Drug Delivery: Case Studies for Cancer and Cardiovascular Applications. *Cell. Mol. Life Sci.* **2012**, 69,389-404.
42. Wang, A.Z.; Langer, R. & Farokhzad, O.C. Nanoparticle Delivery of Cancer Drugs. *Annu. Rev. Med., Vol 63* **2012**, 63,185-198.
43. Shekhar, C. Lean and Mean: Nanoparticle-Based Delivery Improves Performance of Cancer Drugs. *Chem. Biol.* **2009**, 16,349-350.
44. Serdyuk, I.N.; Zaccai, N.R. & Zaccai, G. Methods in Molecular Biophysics : Structure, Dynamics, Function. C.U.P. 2007.
45. Gwladys E. Leclerc, F.C., Ludovic Robert, Marie-Christine, Ho Ba Tho, Colette Rhein, Jean-Paul Latrive, and Sabine F. Bensamoun Analysis of Liver Viscosity Behavior as a Function of Multifrequency Magnetic Resonance Elastography (Mmre) Postprocessing. *J. Magn. Reson. Imaging* **2012**, 38,422-428.
46. Kostarelos, K.; Lacerda, L.; Pastorin, G.; Wu, W.; Wieckowski, S.; Luangsivilay, J.; Godefroy, S.; Pantarotto, D.; Briand, J.P.; Muller, S.; Prato, M. & Bianco, A. Cellular Uptake of Functionalized Carbon Nanotubes Is Independent of Functional Group and Cell Type. *Nat. Nanotechnol.* **2007**, 2,108-113.
47. Lopez, C.F.; Nielsen, S.O.; Moore, P.B. & Klein, M.L. Understanding Nature's Design for a Nanosyringe. *Proc. Natl. Acad. Sci. U. S. A.* **2004**, 101,4431-4434.
48. Wang, X.; Xia, T.; Ntim, S.A.; Ji, Z.; George, S.; Meng, H.; Zhang, H.; Castranova, V.; Mitra, S. & Nel, A.E. Quantitative Techniques for Assessing and Controlling the Dispersion and Biological Effects of Multiwalled Carbon Nanotubes in Mammalian Tissue Culture Cells. *ACS Nano* **2010**, 4,7241-7252.
49. Jeffrey M. Zalc, S.C.R., Enrique Iglesia. Monte-Carlo Simulations of Surface and Gas Phase Diffusion in Complex Porous Structures. *Chem. Eng. Sci.* **2003**, 58,4605–4617.
50. Petersen, E.J.; Huang, Q. & Weber, W.J., Jr. Relevance of Octanol-Water Distribution Measurements to the Potential Ecological Uptake of Multi-Walled Carbon Nanotubes. *Environ. Toxicol. Chem.* **2010**, 29,1106-1112.
51. Spring, K.R. & Hope, A. Size and Shape of the Lateral Intercellular Spaces in a Living Epithelium. *Science* **1978**, 200,54-58.
52. Freitas, R.A. Nanomedicine, Volume I: Basic Capabilities. CRC Press; 1 edition 1999.
53. Judkins, J.; Lee, H.H.; Tung, S. & Kim, J.W. Diffusion of Single-Walled Carbon Nanotube under Physiological Conditions. *J. Biomed. Nanotechnol.* **2013**, 9,1065-1070.
54. Domanov, Y.A.; Aimon, S.; Toombes, G.E.; Renner, M.; Quemeneur, F.; Triller, A.; Turner, M.S. & Bassereau, P. Mobility in Geometrically Confined Membranes. *Proc. Natl. Acad. Sci. U. S. A.* **2011**, 108,12605-12610.
55. Liver Malignancies: Diagnostic and Interventional Radiology (Medical Radiology / Diagnostic Imaging). Softcover reprint of the original 1st ed. 1999 edition, 2012.